



PERGAMON

Journal of Quantitative Spectroscopy &
Radiative Transfer 69 (2001) 245–256

Journal of
Quantitative
Spectroscopy &
Radiative
Transfer

www.elsevier.com/locate/jqsrt

Experimental and theoretical study of the collision-induced fundamental absorption spectra of $\text{N}_2\text{--O}_2$ and $\text{O}_2\text{--N}_2$ pairs

G. Moreau^a, J. Boisssoles^a, R. Le Doucen^a, C. Boulet^b, R.H. Tipping^{c,*}, Q. Ma^d

^aUnité Mixte de Recherche P.A.L.M.S. (Physique des Atomes, Lasers, Molécules, et Surfaces), Université de Rennes I, Campus de Beaulieu, 35042, Rennes Cedex, France

^bLaboratoire de Photophysique Moléculaire, CNRS, Bat. 350, Université de Paris-Sud, Campus d'Orsay, Orsay 91405 Cedex, France

^cDepartment of Physics and Astronomy, University of Alabama, 206 Gallalee, Box 870324, Tuscaloosa, AL 35487-0324, USA

^dDepartment of Applied Physics, Columbia University, and Institute for Space Studies, Goddard Space Flight Center, 2880 Broadway, New York, NY 10025, USA

Received 30 August 1999; accepted 19 May 2000

Abstract

New experimental and theoretical studies of the collision-induced fundamental absorption spectra of $\text{N}_2\text{--O}_2$ and $\text{O}_2\text{--N}_2$ pairs, where the first molecule makes the vibrational transition, are presented for a range of temperatures. Most of the absorption arises from the long-range quadrupolar and hexadecapolar mechanisms for which accurate matrix elements are available from other experimental measurements or from *ab initio* calculations. As in previous studies for $\text{N}_2\text{--N}_2$ and $\text{O}_2\text{--O}_2$, we vary the molecular matrix elements and the coefficients of the short-range induced dipole moments within realistic limits to obtain the best global fit to the temperature-dependent integrated intensities for all the experimental data. This procedure provides a more stringent test of the theory than the previous studies in which the parameters for N_2 and O_2 were optimized independently. Using the parameters thus determined, we then calculate the spectral profiles assuming the line shapes calculated quantum mechanically for N_2 . The agreement between theoretical and experimental profiles is good, but discrepancies in the plateau region of the S-branch, which we attribute to metastable dimer effects, and in the wings of the bands, which we attribute to the neglect of line mixing and higher-order induction mechanisms, still remain. © 2001 Elsevier Science Ltd. All rights reserved.

Keywords: Collision-induced absorption; Oxygen–nitrogen pairs; Fundamental vibration–rotational bands

* Corresponding author. Tel.: + 1-205-348-5050; fax: + 1-205-348-5051.

E-mail address: rtipping@bama.ua.edu (R.H. Tipping).

1. Introduction

In two previous papers, we have carried out theoretical studies of the collision-induced fundamental absorption of $\text{N}_2\text{--N}_2$ and $\text{O}_2\text{--O}_2$ pairs, respectively [1,2]. We considered a number of induction mechanisms characterized by their angular symmetries; these include the dominant long-range quadrupolar induction and the weaker hexadecapolar induction. In the $\text{O}_2\text{--O}_2$ study, we also included the long-range “back reaction” mechanism that, however, produced negligible absorption, and we investigated the effects of including a short-range component for all the various induction mechanisms. In order to calculate the band profiles for both $\text{N}_2\text{--N}_2$ and $\text{O}_2\text{--O}_2$, we used a quantum mechanical line shape calculated for $\text{N}_2\text{--N}_2$ [3] together with matrix elements of the multipole moments and the isotropic and anisotropic polarizability obtained either from independent experimental studies or from accurate *ab initio* calculations. We then varied these quantities by small amounts from their nominal values to obtain the best overall fits to the measured absorptions over a range of temperatures. While the overall agreement between theory and experiment was good, small structural features most apparent the plateau region of the S branch that correspond to dips in the measured profile at the expected line center positions were not present in the theoretically calculated profiles. We attempted to account for these differences in the $\text{O}_2\text{--O}_2$ spectra by modifying the line shape to take into account intercollisional interference [4]. While we could improve the agreement, the density dependence determined was not consistent with that expected for this mechanism. By subtracting the theoretical profile from the experimental data, we obtained residual spectra that resembled dimer spectra observed at lower temperatures [5] and we tentatively identified the small structural features as metastable dimer effects. In addition to the above discrepancies, there were differences in the high- and low-frequency wings of the bands that increased with increasing displacement from the band centers. However, in this region the absorption falls off very rapidly and the experimental errors are large. Higher-order induction mechanisms that would become relatively more important in the wings were not included in the analyses, and the effects of line mixing associated with the anisotropic interaction potential were also ignored.

In the present paper, we present new experimental data for a range of temperatures for the collision-induced absorption in the fundamental regions of $\text{N}_2\text{--O}_2$ and $\text{O}_2\text{--N}_2$ pairs, where the first molecule is the one making the vibrational transition. Because most of the experimental details have been or will be published elsewhere [6–10], we concentrate in this paper on the simultaneous fitting of the fundamental bands for both the pure gases and the mixtures over a wide range of temperatures using the theoretical framework given previously [2]. We determine the values of the matrix elements and magnitudes of the short-range induced dipole moments that yield the best global fit to the experimental data.

The organization of the present paper is as follows. We give in the next section a very brief outline of the theory used in fitting the experimental data. In Section 3, we present comparisons of the theoretical and experimental integrated absorptions, showing the effects of varying the parameters in the theory, and we obtain the best values for the global fit. These results differ slightly from those obtained previously from the independent fits of the fundamental spectra of $\text{N}_2\text{--N}_2$ and $\text{O}_2\text{--O}_2$. We also present comparisons between theoretical and experimental spectral profiles at several temperatures for the gas mixtures using parameters obtained from the global fit. In the final section, we discuss briefly our conclusions from the present work and indicate possible refinements

that could be made to improve the agreement. However, because independent values of the parameters involved in these refinements, for instance, higher-order multipole moment matrix elements or the short-range anisotropic interaction potential, are not known at present, and because the overall agreement without these refinements is reasonably good, we do not feel that it is fruitful at present to introduce additional free parameters simply to improve the fits.

2. Review of the theory

As discussed by Poll and Hunt [11], the spherical components in a space-fixed coordinate system of the induced dipole moment for a pair of molecules can be written quite generally in terms of appropriately coupled spherical harmonics

$$\mu_v(\mathbf{r}_1 \mathbf{r}_2 \mathbf{R}) = [(4\pi)^3/3]^{1/2} \sum_{\lambda_1 \lambda_2 \Lambda L} A_\Lambda(\lambda_1 \lambda_2 L; r_1 r_2 R) \sum_{\mu_1 \mu_2 M} C(\Lambda L 1; \mu_1 + \mu_2, M, v) C(\lambda_1 \lambda_2 \Lambda; \mu_1, \mu_2, \mu_1 + \mu_2) Y_{\lambda_1 \mu_1}(\omega_1) Y_{\lambda_2 \mu_2}(\omega_2) Y_{LM}(\Omega). \quad (1)$$

In this expression, \mathbf{r}_1 ($\equiv r_1, \omega_1$) and \mathbf{r}_2 ($\equiv r_2, \omega_2$) are the vectors describing the orientation of the internuclear axes of molecules 1 and 2, respectively, and \mathbf{R} ($\equiv R, \Omega$) is the vector separation between their centers of mass; the C 's are Clebsch–Gordan coefficients and the Y 's are spherical harmonics. The dipole coefficients, $A_\Lambda(\lambda_1 \lambda_2 L; r_1 r_2 R)$, are real functions of the radial variables and provide a coordinate-independent representation of the strength of the various induction mechanisms specified by the indices $\lambda_1, \lambda_2, \Lambda$ and L . Explicit results for the long-range parts of $A_\Lambda(\lambda_1 \lambda_2 L; r_1 r_2 R)$ arising from back reaction ($L = 1$), quadrupolar ($L = 3$), and hexadecapolar ($L = 5$) induction are given in Table 1. For each component in Table 1, there is also a short-range part that we model by adding a term $\mu_L(r_1, r_2) e^{-(R-\sigma)/\rho}$, where $\mu_L(r_2, r_2)$ for $L = 1, 3, 5$ are adjustable parameters, σ is the Lennard–Jones radius, and ρ is a range parameter which we arbitrarily choose as $\rho = 0.11\sigma$, a value that has been used previously to model H_2 collision-induced spectra.

As in our previous papers [1,2], we neglect the anisotropic interaction between the colliding molecules and write the absorption in terms of a superposition of components. The strengths of the individual components at a temperature T are given by

$$S_j(T) = P_{J_1} C(J_1 \lambda_1 J'_1; 00)^2 P_{J_2} C(J_2 \lambda_2 J'_2; 00)^2 \langle B_n(R)^2 \rangle, \quad (2)$$

in which

$$B_j(R) = \langle v_1 v_2 J_1 J_2 | A_\Lambda(\lambda_1 \lambda_2 L; r_1 r_2 R) | v'_1 v'_2 J'_1 J'_2 \rangle \quad (3)$$

is the matrix element of the coefficient A between the initial and final vibration–rotational states of molecules 1 and 2 assuming simple product-type wavefunctions. The P_J are the normalized Boltzmann factors

$$P_J = g_J(2J + 1) e^{-E_J/kT} / Q(T), \quad (4)$$

Table 1
Induced dipole coefficients

λ_1	λ_2	Λ	L	$A_{\Lambda}(\lambda_1 \lambda_2 L; r_1 r_2 R)$
0	0	0	1	$\frac{6}{5}[\alpha(r_1)\gamma(r_2)Q_2(r_2) - \alpha(r_2)\gamma(r_1)Q_2(r_1)]R^{-7}$
2	0	2	1	$\frac{\sqrt{2}}{5}[(9\alpha(r_1) + 3\gamma(r_1))\alpha(r_2)Q_2(r_1) - \gamma(r_1)\gamma(r_2)Q_2(r_2)/5]R^{-7}$
0	2	2	1	$-\frac{\sqrt{2}}{5}[(9\alpha(r_2) + 3\gamma(r_2))\alpha(r_1)Q_2(r_2) - \gamma(r_1)\gamma(r_2)Q_2(r_1)/5]R^{-7}$
2	0	2	3	$\sqrt{3}[Q_2(r_1)\alpha(r_2)]R^{-4}$
0	2	2	3	$-\sqrt{3}[\alpha(r_1)Q_2(r_2)]R^{-4}$
2	2	2	3	$-(2/105)^{1/2}[Q_2(r_1)\gamma(r_2) - Q_2(r_2)\gamma(r_1)]R^{-4}$
2	2	3	3	$-(2/15)^{1/2}[Q_2(r_1)\gamma(r_2) + Q_2(r_2)\gamma(r_1)]R^{-4}$
2	2	4	3	$-3(2/35)^{1/2}[Q_2(r_1)\gamma(r_2) - Q_2(r_2)\gamma(r_1)]R^{-4}$
4	0	4	5	$\sqrt{5}[Q_4(r_1)\alpha(r_2)]R^{-6}$
0	4	4	5	$-\sqrt{5}[\alpha(r_1)Q_4(r_2)]R^{-6}$
4	2	4	5	$-2/3(7/55)^{1/2}[Q_4(r_1)\gamma(r_2)]R^{-6}$
4	2	5	5	$-2(1/15)^{1/2}[Q_4(r_1)\gamma(r_2)]R^{-6}$
4	2	6	5	$-(26/33)^{1/2}[Q_4(r_1)\gamma(r_2)]R^{-6}$
2	4	4	5	$2/3(7/55)^{1/2}[\gamma(r_1)Q_4(r_2)]R^{-6}$
2	4	5	5	$-2(1/15)^{1/2}[\gamma(r_1)Q_4(r_2)]R^{-6}$
2	4	6	5	$(26/33)^{1/2}[\gamma(r_1)Q_4(r_2)]R^{-6}$

where

$$Q(T) = \sum_J g_J (2J + 1) e^{-E_J/kT}, \quad (5)$$

and g_J are the nuclear statistical weights. Therefore, using the explicit results for the induction coefficients $A_{\Lambda}(\lambda_1 \lambda_2 L; r_1 r_2 R)$ listed in Table 1, we can write the $B_n(R)$ in the form

$$B_j(R) = \langle 00J_1 J_2 | A_{\Lambda}(\lambda_1 \lambda_2 L; r_1 r_2) | 01J'_1 J'_2 \rangle R^{-(L+1+5\delta_{L1})}, \quad (6)$$

where δ_{L1} is the Kronecker delta. The average over molecular orientations, denoted by angular brackets, can be calculated using the well-known results

$$\langle B_j(R)^2 \rangle = 4\pi \int_0^{\infty} B_j(R)^2 g(R) R^2 dR, \quad (7)$$

where $g(R)$ is the pair distribution function approximated by

$$g(R) = e^{-V_0(R)/kT}. \quad (8)$$

We assume that the isotropic potential $V_0(R)$ can be adequately represented by a Lennard–Jones potential, whose values of ε and σ are obtained from those of the pure gases [1,2] by the usual combining rules, viz., $\sigma_{ij} = (\sigma_{ii} + \sigma_{jj})/2$ and $\varepsilon_{ij} = (\varepsilon_{ii} \varepsilon_{jj})^{1/2}$. Furthermore, if we neglect the slight

dependence of the matrix elements in Eq. (6) on the rotational quantum numbers, we can approximate Eq. (7) by

$$\langle B_j(R)^2 \rangle \cong |\langle 0000 | A_\Lambda(\lambda_1 \lambda_2 L; r_1 r_2) | 0100 \rangle|^2 I(L), \quad (9)$$

where

$$I(L) = 4\pi \int_0^\infty R^{-2} (L + 5\delta_{L1}) e^{-V_o(R)/kT} dR, \quad (10)$$

and $L = 1, 3$ or 5 for the back, quadrupolar, and hexadecapolar induction mechanisms, respectively. Then summing up the various components j listed in Table 1, we can calculate the integrated intensity, or by multiplying each component by the normalized line-shape function, $L_j(\omega - \omega_{if})$, at its appropriate absorption frequency, ω_{ij} , computed from the gas values of the spectroscopic constants, we can compute the spectral band profiles for the mixtures from

$$A(\omega, T) \equiv \alpha(\omega)/\rho_{N_2} \rho_{O_2} = (4\pi^2/3) \alpha_F n_0^2 a_0^5 \omega \sum_{\substack{j, J_1, J'_1 \\ J_2, J_2}} S_j(T) L_j(\omega - \omega_{if}). \quad (11)$$

Here α_F is the fine structure constant, n_0 is the number density at normal temperature and pressure, and a_0 is the Bohr radius.

3. Comparison between theory and experiment

As a first step, we calculated the zeroth moment of the spectra [4]

$$\gamma_0 = \int A(\omega, T) \omega^{-1} d\omega \quad (12)$$

for the fundamental bands of pure N_2 , pure O_2 , and for O_2 – N_2 and N_2 – O_2 mixtures as a function of temperature T using the values found previously [1,2] for the various molecular parameters; these are listed in column 1 of Table 2. The results for N_2 and O_2 denoted by the symbol + — + are shown in Figs. 1 and 2 along with the experimental data and 5% errors bars [6–10]. Some of these data have not been published previously; specifically that of Moreau [10] for N_2 – N_2 and O_2 – O_2 , and that of Lafferty et al. [12] for O_2 – O_2 . The zeroth moment for the mixtures N_2 – O_2 and O_2 – N_2 using these molecular parameters are shown in Figs. 3 and 4, respectively, together with previously published [7,9] and new experimental data of Moreau [10] and Lafferty et al. [12]. As can be seen from these figures, we obtain reasonable results for O_2 – N_2 but are considerably outside of the error bars for N_2 – O_2 . We then tried to vary the two parameters that account for the dominant contribution to the absorption, viz., α_{00} and Q_{01} for both O_2 and N_2 . The results denoted by the symbol < | — < | for the 4 cases shown in Figs. 1–4 are calculated using the values listed in column 2 of Table 2. While the overall agreement is improved, large discrepancies still remain. As a second step, we varied α_{00} , Q_{01} and the Lennard–Jones radii, σ_{N_2} and σ_{O_2} (and thus σ for the mixtures), which affect both the isotropic potential, V_0 , and the

Table 2
Molecular parameters in atomic units

N_2			
α_{00}	11.74	11.50	11.50
α_{01}	0.365	0.365	0.365
γ_{00}	4.75	4.75	4.75
γ_{01}	0.438	0.438	0.438
Q_{00}	-1.052	-1.052	-1.052
Q_{01}	5.63×10^{-2}	6.13×10^{-2}	6.13×10^{-2}
ϕ_{00}	-7.5	-7.5	-7.5
ϕ_{01}	-1.5×10^{-1}	-1.5×10^{-1}	-1.5×10^{-1}
σ	6.956	6.956	7.005
O_2			
α_{00}	10.87	11.08	11.08
α_{01}	0.357	0.357	0.357
γ_{00}	7.30	7.30	7.30
γ_{01}	0.57	0.57	0.57
Q_{00}	-0.264	-0.264	-0.264
Q_{01}	0.106	0.1028	0.1028
ϕ_{00}	4.4	4.4	4.4
ϕ_{01}	0.185	0.185	0.185
σ	6.55	6.55	6.435

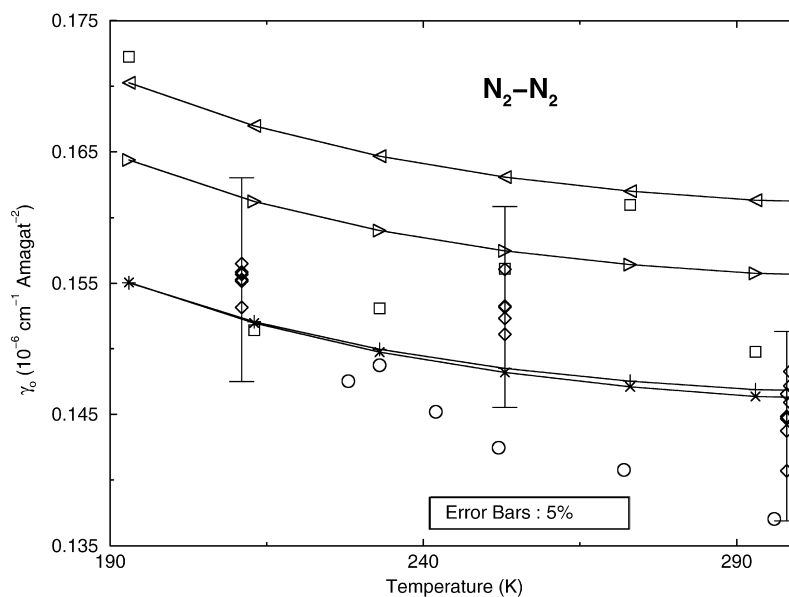


Fig. 1. The temperature dependence of the zeroth moment of the fundamental band of N_2-N_2 . Experimental results: \circ Ref. [8]; \square Ref. [6]; \diamond Ref. [10]. Theoretical results: $+ \text{---} +$ calculated with the values in column 1 of Table 2; $<| \text{---} |>$ calculated with the values given in column 2 of Table 2; $|> \text{---} |>$ calculated with the values given in column 3 of Table 2; $* \text{---} *$ calculated with the values given in column 3 of Table 2 including the short-range quadrupole-induced dipole contributions.

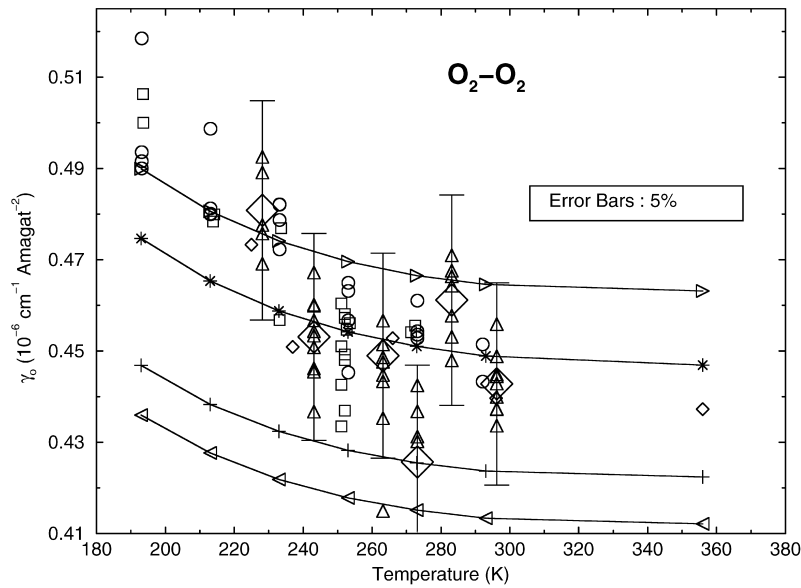


Fig. 2. The same as Fig. 1 for $\text{O}_2\text{--O}_2$. Experimental results: \circ Ref. [7]; \square Ref. [10]; \triangle Ref. [12]; \diamond Ref. [12].

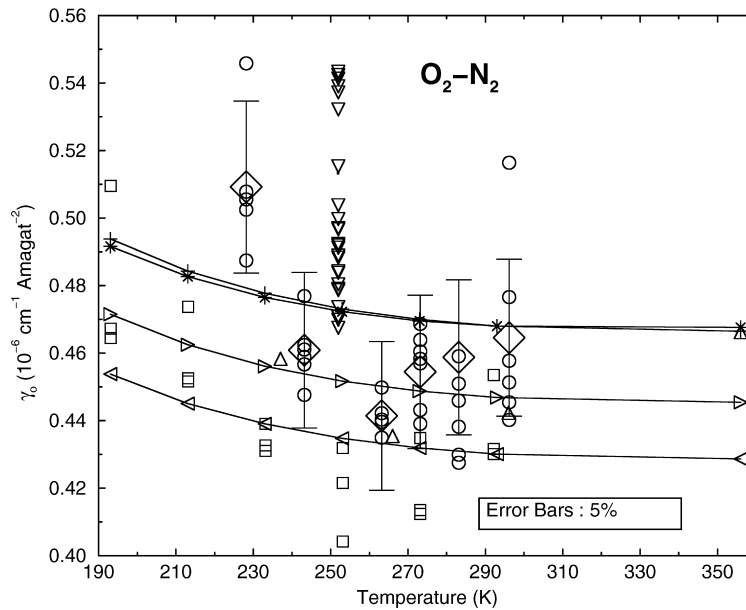


Fig. 3. The same as Fig. 1 for $\text{O}_2\text{--N}_2$. Experimental results: \circ Ref. [12]; \triangle Ref. [9]; \square Ref. [7]; ∇ Ref. [10].

short-range functional form of the induced dipole function. The values are given in column 3 of Table 2 and the results are shown in Figs. 1–4 by the symbol $|> \text{---}|>$. Finally, we considered a short-range contribution to the dominant quadrupolar induction mechanism. Letting $N_2 \equiv 1$

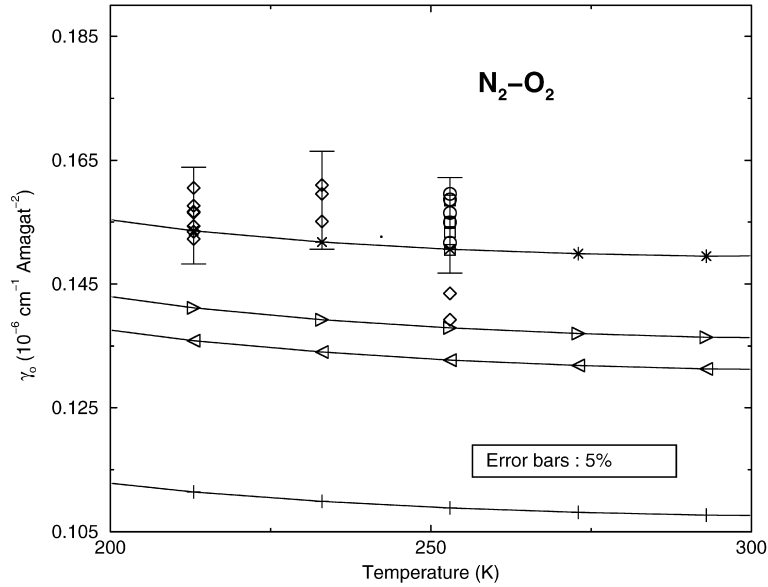


Fig. 4. The same as Fig. 1 for $\text{N}_2\text{-O}_2$. Experimental results are all from Ref. [10] for three independent measurements.

and $\text{O}_2 \equiv 2$, this dipole component (ignoring the angular dependence) is of the form

$$\mu_v = \sqrt{3}\{Q_2(r_1)\alpha(r_2) - \alpha(r_1)Q_2(r_2)\} \pm \mu_3(r_1, r_2)e^{-(R-\sigma)/\rho}, \quad (13)$$

where $\mu_3(r_1, r_2) = \mu'_3(r_1 - r_2) + \dots$ and μ'_3 is an adjustable parameter. This form satisfies the symmetry requirement that interchange of r_1 and r_2 changes the direction of the dipole and one gets a minus sign. We do not know whether the short-range coefficient is $+$ or $-$, nor do we know the sign of μ'_3 . For the $\text{N}_2\text{-O}_2$ spectrum, we have to consider the $\langle 0|\langle 0|\mu_v|1\rangle|0\rangle$ vibrational matrix element, and for the $\text{O}_2\text{-N}_2$ spectrum, we have to consider the $\langle 0|\langle 0|\mu_v|0\rangle|1\rangle$ matrix element. In the first case, the dominant term is $Q_{01}\alpha_{00}$ (this is larger than $\alpha_{01}Q_{00}$), while in the second case it is $-\alpha_{00}Q_{01}$, thus introducing a minus sign. Since $\langle 0|\langle 0|r_1 - r_2|1\rangle|0\rangle = \langle 0|r_1|1\rangle - \langle 0|r_2|0\rangle \cong -r_{2e}$ while $\langle 0|\langle 0|r_1 - r_2|0\rangle|1\rangle = \langle 0|r_1|0\rangle - \langle 0|r_2|1\rangle \cong r_{1e}$, these also differ in sign. Therefore, the interference in $\text{O}_2\text{-N}_2$ and $\text{N}_2\text{-O}_2$ should have the same overall sign, and the magnitude for $\text{N}_2\text{-O}_2$ should be approximately 10% larger than that for $\text{O}_2\text{-N}_2$, reflecting the ratio of equilibrium internuclear separations in O_2 and N_2 . For pure O_2 or N_2 , the function $\mu_3(r_1, r_2)$ can be different in sign and magnitude from the mixtures because they arise from $\text{O}_2\text{-O}_2$ or $\text{N}_2\text{-N}_2$ collisions; in these cases, one can have resonant collisions, exchange symmetry, etc.

We find that the results using $\mu'_3 r_e = -5.0 \times 10^{-5}$ for $\text{N}_2\text{-O}_2$, -4.5×10^{-5} for $\text{O}_2\text{-N}_2$, and $\mu'_3 r_e = 5.0 \times 10^{-5}$ for $\text{O}_2\text{-O}_2$ and $\text{N}_2\text{-N}_2$, together with the parameters in column 3 of Table 2 give reasonable global fits to all the data; these are shown in Figs. 1–4, denoted by the symbol *—*. Without accurate ab initio calculations, the magnitudes and signs of the short-range fitting parameters cannot be independently verified at present. Although the isotropic

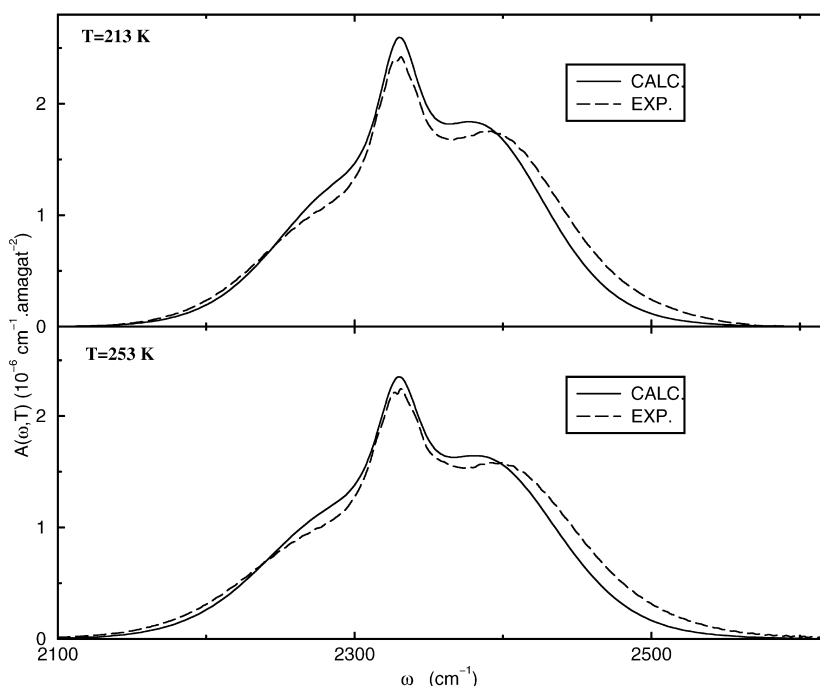


Fig. 5. Comparison between theory and experimental values from Ref. [10] for the absorption coefficient (in units $10^6 \text{ cm}^{-1} \text{ amagat}^{-2}$ versus frequency ω in cm^{-1} for the $\text{N}_2\text{-O}_2$ fundamental band: (a) $T = 213 \text{ K}$; (b) $T = 253 \text{ K}$.

polarizability matrix elements of N_2 and O_2 are similar, the matrix elements of the other parameters are considerably different in magnitudes and signs as can be seen from Table 2. Thus, one could expect significant differences in the short-range induced dipoles, especially in their dependence on the internuclear separation implicit in μ'_3 .

Finally, using the set of parameters that gave the best global fit to the zero'th moments, one can easily compute the corresponding spectral profiles. Sample results for the mixtures are presented in Figs. 5 and 6 for several temperatures. Similar results obtain for the pure gases and for other temperatures for the mixtures.

4. Discussion and conclusions

As evident from the figures, one can obtain a reasonable global fit to the fundamental spectra of $\text{N}_2\text{-N}_2$, $\text{O}_2\text{-O}_2$, $\text{N}_2\text{-O}_2$, and $\text{O}_2\text{-N}_2$ over a range of temperatures using the theory outlined in Section 2. The parameters obtained for the matrix elements of the multipole moments, isotropic, and anisotropic polarizabilities differ by ± 2 to 3% from those obtained from other experiments or from ab initio calculations that were used previously in the pure gas cases [1,2], except for the value of Q_{01} of N_2 . The value found in the present work is approximately 9% higher than the value we used previously [13]; however, we note that three other experimental determinations were also all larger, the largest by 4% [14]. Furthermore, a more recent ab initio calculation [15,16] obtained

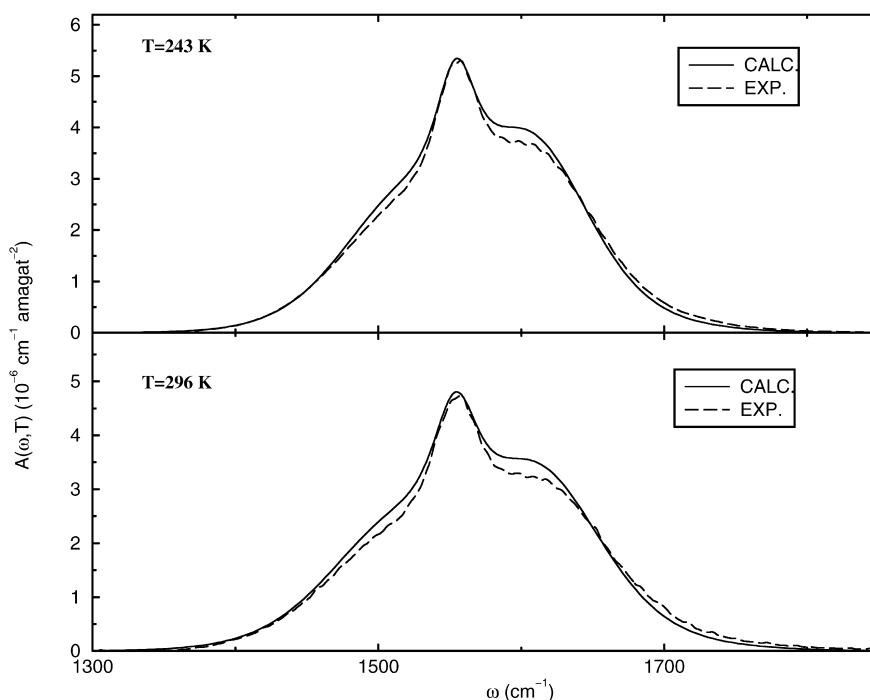


Fig. 6. Comparison between theory and experimental values from Ref. [12] for the absorption coefficient (in units $10^6 \text{ cm}^{-1} \text{ amagat}^{-2}$) versus frequency ω in cm^{-1} for the $\text{O}_2\text{--N}_2$ fundamental band: (a) $T = 243 \text{ K}$; (b) $T = 296 \text{ K}$.

the value $Q_{01} = 0.065 a_0$ which is significantly higher than both previous experimental values and the value obtained by our fitting. (We note that the minus sign in Ref. [16] results from their choice of phase of the $v = 1$ wave function. Because the derivative $(\partial Q / \partial r)_r > 0$, the fundamental matrix element should be positive.)

To achieve an acceptable global fit, it was necessary to add a short-range component to the dominant quadrupolar induction mechanism. The magnitude of this component is reasonable when compared with similar quantities in H_2 [17]. In the present work, we did not use the line shape model containing a dip at the center due to intercollisional interference [2]; therefore, there are small structural differences apparent in the plateau region of the S branch as in previous works [1,2]. A more detailed treatment of these features attributable to metastable–metastable transitions in dimers will be published elsewhere [18]. In addition, there are differences between theory and experiment in the wings of the bands. As mentioned previously, one can get more absorption in the wings by including higher-order induction mechanisms, with the concomitant introduction of additional parameters. Moreover, one should also take into account the phenomena of line mixing [19]. In the previous work as well as the present, we have neglected the effects of the anisotropic interaction, thus enabling us to obtain the band profile as a simple superposition of individual line contributions. This simplification affects the band profile in the collision-induced spectra in a way similar to allowed spectra [19]. That is, one would expect some of the intensity in the wings to be transferred closer to the band center. While the above-mentioned refinements could be made, it is

worth keeping in mind that there are considerable experimental uncertainties in the wings due to the inherent weakness of the induced spectra.

One final point deserves mention. Using the parameters obtained in the present study, we have also calculated the double vibrational collision-induced absorption. The magnitude of the integrated intensity at room temperature is approximately $5.6 \times 10^{-10} \text{ cm}^{-2} \text{ cm}^{-2}$. Because this absorption occurs at the sum of the fundamental frequencies of N_2 and O_2 , it is well separated from both of the overtone regions of pure N_2 or pure O_2 . A measurement of this spectral region, preferably with a 50–50 mixture of N_2 and O_2 , would further verify the parameters obtained in the present study.

Acknowledgements

The authors would like to thank Walter Lafferty for providing his experimental data prior to publication. Two of the authors (RHT and QM) would like to acknowledge support from NASA through Grants NAG5–6314 and NAG5–8269, and of the three authors (CB, RHT, and QM) wish to thank NATO for an exchange Grant (CRG 940247) during which this research was begun.

References

- [1] Boissolles J, Tipping RH, Boulet C. Theoretical study of the collision-induced fundamental absorption spectra of N_2 – N_2 pairs for temperatures between 77 K and 297 K. *JQSRT* 1994;51:615–27.
- [2] Moreau G, Boissolles J, Boulet C, Tipping RH, Ma Q. Theoretical study of the collision-induced fundamental absorption spectra of O_2 – O_2 pairs for temperatures between 193 K and 273 K. *JQSRT* 2000;64:87–107.
- [3] Borysow A, Frommhold L. Collision-induced rototranslational absorption spectra of N_2 – N_2 pairs for temperatures from 50 to 300 K. *Astrophys J* 1986;311:1043–57.
- [4] Frommhold L. Collision-induced absorption in gases.. Cambridge: Cambridge University Press, 1993.
- [5] McKellar ARW. Infrared spectra of the $(\text{N}_2)_2$ and N_2 –Ar van der Waals molecules. *J Chem Phys* 1988; 88:4190–6.
- [6] Menoux V, Le Doucen R, Boulet C, Roblin A, Bouchardy Am. Collision-induced absorption in the fundamental band of N_2 : temperature dependence of the absorption for N_2 – N_2 and N_2 – O_2 pairs. *Appl Opt* 1993;32:263–8.
- [7] Thibault F, Menoux V, Le Doucen R, Rosenmann L, Hartmann J-M, Boulet C. Infrared collision-induced absorption by O_2 near 6.4 μm for atmospheric applications: measurements and empirical modeling. *Appl Opt* 1997;36:1–5.
- [8] Lafferty WJ, Solodov AM, Weber A, Olson WB, Hartmann J-M. Infrared collision-induced absorption by N_2 near 4.3 μm for atmospheric applications: measurements and empirical modeling. *Appl Opt* 1996;35:5911–7.
- [9] Orlando JJ, Tyndall GS, Nickerson KE, Calvert JG. The temperature dependence of collision-induced absorption by oxygen near 6 μm . *J Geophys Res* 1991;96:20755–60.
- [10] Moreau G. Etude expérimentale et théorique des spectres induits par collision de N_2 – N_2 , N_2 – O_2 , O_2 – O_2 , et O_2 – N_2 , dissertation, Université de Rennes, 1999.
- [11] Poll J, Hunt J. On the moments of the pressure-induced spectra of gases. *Can J Phys* 1976;54:461–74.
- [12] Maté B, Luyez CL, Solodov AM, Fraser GT, Lafferty WJ. Investigation of the collision-induced absorption by O_2 near 6.4 μm in pure O_2 and O_2/N_2 mixtures. *J Geophys Res* 2000;105:22,225–30.
- [13] Reuter D, Jennings DE, Brault JW. The $\nu = 1 < -0$ Quadrupole Spectrum of N_2 . *J Mol Spectrosc* 1986;115:294–304.
- [14] Guelachvili G, Narahari RK. Handbook of infrared standards.. Orlando, FL: Academic Press, 1986.
- [15] Piecuch P, Kondo AE, Spirko V, Paldus J. Molecular quadrupolar functions of HF and N_2 . I. Ab initio linear-response coupled-cluster results. *J Chem Phys* 1996;104:4699–715.

- [16] Spirko V, Picuch P, Kondo AE, Paldus J. Molecular quadrupolar functions of HF and N₂. II. Rovibrational effects. *J Chem Phys* 1996;104:4716–27.
- [17] Meyer W, Borysow A, Frommhold L. Absorption spectra of H₂–H₂ pairs in the far infrared. *Phys Rev A* 1989;40:6931–49.
- [18] Moreau G, Boissoles J, Le Doucen R, Boulet C, Tipping RH, Ma Q. Metastable dimer contributions to the collision-induced fundamental absorption spectra of N₂ and O₂ pairs. *JQSRT*. In press.
- [19] Levy A, Lacome N, Chackerian Jr. C. Collisional line mixing.. In: Rao KN, Weber A, editors. *Spectroscopy of the earth's atmosphere and interstellar medium..* Boston: Academic Press, 1992, p. 261–337.